condensed matter

MDPI

Article

Effect of the Strength of Attraction Between Nanoparticles on Wormlike Micelle-Nanoparticle System

Mubeena Shaikh

IISER-Pune, Dr. Homi Bhabha Road, Pune 411008, India; mubeena@students.iiserpune.ac.in; Tel.: +91-913-0731-891

Received: 31 August 2018; Accepted: 10 October 2018; Published: 13 October 2018

Abstract: The nanoparticle-Equilibrium polymer (or Wormlike micellar) system shows morphological changes from percolating network-like structures to non-percolating clusters with a change in the minimum approaching distance (EVP-excluded volume parameter) between nanoparticles and the matrix of equilibrium polymers. The shape anisotropy of nanoparticle clusters can be controlled by changing the polymer density. In this paper, the synergistic self-assembly of nanoparticles inside equilibrium polymeric matrix (or Wormlike micellar matrix) is investigated with respect to the change in the strength of attractive interaction between nanoparticles. A shift in the point of morphological transformation of the system to lower values of EVP as a result of a decrease in the strength of the attractive nanoparticle interaction is reported. We show that the absence of the attractive interaction between nanoparticles leads to the low packing of nanoparticle structures, but does not change the morphological behavior of the system. We also report the formation of the system spanning sheet-like arrangement of nanoparticles which are arranged in alternate layers of matrix polymers and nanoparticles.

Keywords: self-assembly; polymer nanocomposites; polymer templating; equilibrium polymers; Wormlike micelles; mesoporous structures; bottom-up approach

1. Introduction

Nanostructures have a wide range of applications in energy devices [1,2], optoelectronic devices [3], drug delivery [4–6], cosmetics [7,8], food [9,10] and novel functional materials [11,12]. To produce nanostructures, the bottom-up approach has recently become a cost-effective and easy method in the nanofabrication industry [13,14]. Using polymeric matrices to assemble nanoparticles is one of the prominent methods in bottom-up approach [15–18], e.g., production of various nanostructures using di-block copolymers matrix [19]. However, tailoring nanostructures with a precise control over their size and shape is a challenge in nanofabrication industry.

Polymer nanocomposites (PNCs) form an active research field with a variety of theoretical and simulation techniques to get an insight into the structure-property relationship. The early equilibrium theoretical studies [20,21] integrate out the polymer degree of freedom while recent theories have be developed to take into account the degrees of freedom of both the particles and the polymers. Fredrickson and co-workers [22,23] used a self-consistent field theory framework to study the nanoparticle assembly in a self-assembled block copolymers [24–26] and a more generalized version was presented later by Riggleman and co-workers [27,28]. This was further developed by Balazs [29–31] and Frischknecht [32–34] to apply it to both homo and block copolymers matrices. There also exists simulation techniques developed by de Pablo [35–37] or a soft particle approach by Bolhuis and co-workers [38–40]. Despite such advances in the filed of PNCs, there exists significant gaps in understanding the PNC systems and their structure–property relationship.

In this paper, we employ equilibrium polymeric matrix (or Wormlike micellar matrix) to self-assemble nanoparticles into various kind of structures and investigate the effect of the strength of nanoparticle interaction. Nanoparticles with their high surface to volume ratio make it difficult to disperse them in a polymeric matrix. Therefore, nanoparticles are often grafted by polymers or have a surface modification to get a homogenous dispersion [41]. The assembly of such grafted nanoparticles in a polymeric matrix depends on the ratio of the size of nanoparticle core to the grafted polymer [42], polydispersity of the graft lengths [43,44], distribution of grafted chains on the nanoparticle surface [45], the grafting method [46], etc. Apart from the dispersion of nanoparticles in a matrix, it is also important to study the effect of interaction between nanoparticles to get a precise control over tailoring nanostructures with desired properties and shape.

The nanoparticles self-assemble in an equilibrium polymeric matrix to give rise to various kind of structures, viz. mesoporous networks, nanorods and nanosheets [47]. With an increase in minimum approaching distance between nanoparticles and polymers (EVP, excluded volume parameter), a morphological transition of nanoparticles from network-like structures to individual clusters has been shown in a previous study [47]. The study also indicates that we can control the anisotropy of the nanoparticle clusters by tuning the density of the matrix. In this paper, we report the shift in the values of the EVP required for the structural change of nanoparticles, as a result of the change in the strength of nanoparticle interaction. We also report a decrease in the packing of nanoclusters with a decrease in the strength of attractive interaction between them. Moreover, the formation of the system spanning nanoparticle sheets is also observed.

2. Model and Method

2.1. Modeling Wormlike Micelles

The model used in this paper is the same as the model used in [47,48] which is a modified version of the model presented in [49]. According to this model, the Wormlike micellar chains are coarse-grained as a chain of spherical beads. Each spherical bead (here called as monomer) in the model is assumed to represent a group of amphiphilic molecules at the mesoscopic scale. All the chemical details are ignored here and only the relevant details to describe behavior at the mesoscopic scale are considered. The schematic diagram of the model is shown in Figure 1a. The spheres represent the monomers of size σ, which we set as the unit of length in the system. All distances are shown with respect to the central monomer (shown in pink). These monomers are allowed to interact with each other using three potentials, a two-body V_2, three-body V_3 and a four-body potential V_4. The behavior of the three potentials is shown in Figure 1b and the potentials are expressed as follows,

- V_2**: Two body attractive potential**
  For any two monomers at a distance of r_2, an attractive Lennard–Jones potential is provided which is modified by an exponential term as shown in Equation (1).

$$V_2 = \epsilon[(\frac{\sigma}{r_2})^{12} - (\frac{\sigma}{r_2})^6 + \epsilon_1 e^{-ar_2/\sigma}]; \forall r_2 < r_c. \quad (1)$$

  where $\epsilon = 110k_BT$ and the cutoff distance is $r_c = 2.5\sigma$. The exponential term in the above potential creates a maximum at $r_2 = 1.75\sigma$ which acts as a potential barrier for joining or breaking of monomers from chains. The value of ϵ_1 and a are kept fixed as $\epsilon_1 = 1.34\epsilon$ and $a = 1.72$. This potential behavior is shown in Figure 1b where the Y-axis is $V_2 + V_3$. When $\theta = 0$, $V_3 = 0$ (see below). Therefore, the graph shown by the symbols (blue-triangle) having legends $\sin^2\theta = 0$ represents the behavior of V_2. In the graph, r_2 is kept fixed at $r_2 = \sigma$ (except for the inset figure).
- V_3**: Three body potential to add semi-flexibility to chains**

For any monomer that is part of a chain, there are two bonded neighbours at a distance of r_3 and r_4 which subtends an angle θ at the central monomer (as shown in Figure 1). The triplet thus formed is then subjected to the following three-body potential,

$$V_3 = \epsilon_3(1 - \frac{r_2}{\sigma_3})^2(1 - \frac{r_3}{\sigma_3})^2 \sin^2(\theta); \forall r_2, r_3 < \sigma_3. \quad (2)$$

where the value of $\epsilon_3 = 6075 k_B T$ and the cutoff distance σ_3 is kept fixed at 1.5σ. The leading terms inside the two brackets ensure that the potential and force goes smoothly to zero at the cutoff of σ_3.

- V_4**: Four body repulsive potential between chains**
  For any monomer with two bonded neighbours at distances r_2 and r_3, any other monomer at a distance r_4 approaching the first monomer to form a branch (see Figure 1a) will be repelled with the following potential,

$$V_4 = \epsilon_4(1 - \frac{r_2}{\sigma_3})^2(1 - \frac{r_3}{\sigma_3})^2 \times V_{LJ}(\sigma_4, r_4) \quad (3)$$

The cutoff distance for this potential σ_4 is chosen such that $\sigma_3 < \sigma_4 < r_c$ and is fixed at $\sigma_4 = 1.75\sigma$. The leading terms in the brackets are necessary to make the force and potential smoothly approaching zero at the cutoff distance. Since, those terms in the brackets approaches zero as r_2 or r_3 approaches σ_3, therefore the value of ϵ_4 is decided to give a very high value $\epsilon_4 = 2.53 \times 10^5\ k_B T$ to ensure enough repulsion between the chains. The behavior of V_4 is shown in the inset of Figure 1b. It should be noted that we refer to micellar chains as dispersed if the distance between chains is $> 1.75\sigma$. When the distance between chains of monomers is $< 1.75\sigma$, then we refer to them as clusters of chains.

Using Monte Carlo technique, the system is allowed to equilibrate from a randomly initialized state. After around $5 \times 10^5 - 6 \times 10^5$ iterations, the system evolves to form Wormlike chains of monomers having an exponential distribution of chain length [48]. With an increase in micellar density, an isotropic-to-nematic transition is observed, as has been reported in detail [48].

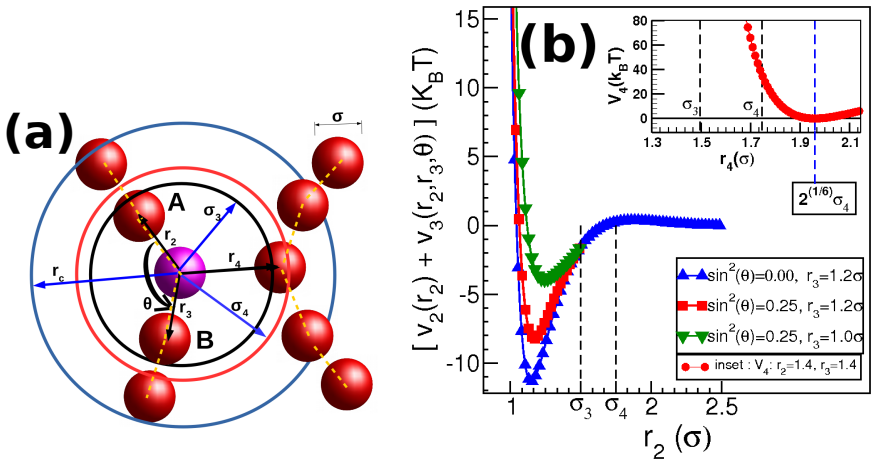

Figure 1. The figure shows the modeling of the Wormlike micelles. The spheres denote the micellar monomers having diameter σ. All the distances are measured with respect to the central monomer shown in pink. These monomers are acted upon by two body potential V_2 having a cutoff range of r_c. A three-body potential V_3 is acting on a triplet with a central monomer (pink) bonded with two other monomers at distances of r_2 and r_3, forming an angle θ at the central monomer and having a cutoff range of σ_3. In addition to these potentials, there exists a four-body potential V_4 which is a shifted Lennard–Jones potential introduced to prevent branching and having a cutoff distance $2^{1/6}\sigma_4$.

2.2. Modeling Nanoparticles

To investigate the phase behavior of Wormlike micelle-nanoparticle system, model nanoparticles are added in the model Wormlike micellar system described in the above section. Nanoparticles are modeled by Lennard–Jones attractive particles of size σ_n and having a cutoff distance r_{cn} with the interacting potential V_{2n} given by,

$$V_{2n} = \epsilon_n[(\frac{\sigma_n}{r_n})^{12} - (\frac{\sigma_n}{r_n})^6], \forall r_n <= r_{cn} \quad (4)$$

The cutoff distance r_{cn} is set at $r_{cn} = 2\sigma_n$. These nanoparticles interact with monomers via a repelling potential V_{4n} which is a shifted Lennard–Jones potential given by,

$$V_{4n} = \epsilon_{4n}[(\frac{\sigma_{4n}}{r_{mn}})^{12} - (\frac{\sigma_{4n}}{r_{mn}})^6], \forall r_{mn} <= 2^{1/6}\sigma_{4n} \quad (5)$$

where r_{mn} indicates the distance between monomers and nanoparticles with the parameter σ_{4n} indicating the centre-to-centre distance between the particles. The value of σ_{4n} is used as a parameter. The value of the strength of the repulsive interaction is fixed at $\epsilon_{4n} = 30k_BT$.

In summary, in this model (refer Figure 1a), there are coarse-grained particles (spheres) to form micellar chains of the size σ that interacts with each other via a Lennard–Jones potential having a cutoff distance 2.5σ. The micellar chains are semi-flexible (potential V_3) and repel each other with the potential V_4 and the minimum approaching distance $\sigma_4 = 1.75\sigma$. The system also contains nanoparticles of size σ_n which are interacting by a Lennard–Jones attractive potential among themselves (potential V_{2n}) with a cutoff distance $2\sigma_n$. These monomers and nanoparticles are repelled by a repulsive potential V_{4n} with the minimum approaching distance σ_{4n} and cutoff distance $2^{1/6}\sigma_{4n}$. The value of σ_{4n} is used as a parameter.

Using this model, the morphological transformations of the system with a change in σ_{4n} and micellar density has been established [47] (keeping the nanoparticle size fixed at $\sigma_n = 1.5\sigma$). Now, in this paper, the system is investigated to explore the effect of the strength of the attractive interaction between nanoparticles ϵ_n on the system behavior. Therefore, we keep the nanoparticle size fixed at $\sigma_n = 1.5\sigma$, while using ϵ_n as a variable along with σ_{4n} and the number density of monomers ρ_m. We generate runs in sets where each set consists of runs with a fixed ϵ_n but σ_{4n} and ρ_m as parameters.

2.3. Method

The model is first applied with the Metropolis Monte Carlo (MC) method. However, the method seemed to be insufficient to equilibrate the system with high density. Therefore, the system is first evolved with Metropolis Monte Carlo method with 200–300 nanoparticles within a given number density of monomers ρ_m for 10^5 iterations. This gives the monomers enough time to develop into chain-like structures in the presence of seeding of nanoparticles. Then, a semi-grand canonical Monte Carlo (GCMC) scheme is applied. According to this scheme, for every 50 Monte Carlo steps, 300 attempts are made to add and remove a nanoparticle randomly. Each successful attempt is penalized with an energy gain or loss of $\pm\ \mu_n$, where, μ_n is the chemical potential of the system fixed at $\mu_n = -8\ k_BT$. All runs were tested with ten independent runs which show convergence to morphologically similar states and their thermodynamic properties converging to the same values. It is shown that, for the model system, runs that started with an unmixed state (both nanoparticles and monomers separated) also tend to form a mixed state for the value of μ_n chosen. Thus, the possibility of a fully phase separated state as a thermodynamically preferred state is negated [47].

For all the runs in this paper, we first apply the Metropolis Monte Carlo method to allow the growth of equilibrium polymeric chains in the presence of seed of nanoparticles. Then, GCMC scheme is switched on for the rest of the run. For each set of parameters, the system is evolved for $\approx\ 20 \times 10^5 - 40 \times 10^5$ iterations and the thermodynamic properties are averaged for the last

$10 \times 10^5 - 20 \times 10^5$ iterations over ten independent runs. The error bars in the plots shown in this paper are smaller than the symbols and hence not visible here.

3. Results

Previous studies [47,48] using the same model (presented in the previous section) have reported the morphological transitions of nanoparticles with the increase in σ_{4n}. Those results were substantiated by showing the convergence of all ten independent runs to same morphological structures. It is emphasized here that all these studies are comprised of systems that are initialized with a mixed state of nanoparticles and micelles. It was shown that the nanoparticle clusters formed in the system vary in their shape anisotropy with a change in matrix polymer density. This paper takes this investigation further by varying the strength of interaction between nanoparticles ϵ_n along with σ_{4n} and monomer No. density ρ_m. All quantities calculated are averaged over ten independent runs.

To investigate the effect of the strength of interaction between nanoparticles ϵ_n, a set of runs varying in the value of ρ_m and σ_{4n} is generated for each value of ϵ_n. For a given value of ϵ_n, the system morphological behavior is observed and the structural changes are identified. Then, these structural changes are compared over different values of ϵ_n and the change in the value of EVP at which the morphological change occurs are observed. Different values of $\epsilon_n = 2k_BT, 5k_BT, 8k_BT$ and $11k_BT$ are considered. Apart from these values, one more case where there exists no attractive interaction between nanoparticles is also considered. In this case, the nanoparticles are provided with WAC (Week–Anderson–Chandler) potential (similar to the potential expressed in Equation (5). We represent this case by $\epsilon_n = 0$ only for convenience. For each value of ϵ_n, a set of runs with four values of number density of monomers $\rho_m = 0.037\sigma^{-3}$, $0.074\sigma^{-3}$, $0.093\sigma^{-3}$ and $0.126\sigma^{-3}$, along with varying parameter σ_{4n} for each density, are produced. The system is evolved using MC steps for first 10^5 iterations and then subjected to GCMC scheme for the rest of the iterations. The system is monitored to ensure that the runs are long enough to produce structures and thermodynamic quantities that are stable over a long run. After around $2 \times 10^5 - 3 \times 10^5$ iterations, the systems are observed to maintain their morphological states. The behavior of the average energy of the particles for $\rho_m = 0.037\sigma^{-3}$ is shown in Figure 2 for two different values of ϵ_n: (a) 0; and (b) $2k_BT$. For each value of ϵ_n, the figure shows graphs for four different values of $\sigma_{4n} = 1.5\sigma, 1.75\sigma, 2\sigma$ and 2.25σ. In both figures, all graphs show a jump in their energy values at 10^5 Monte Carlo Steps (MCSs). These jumps mark the starting of the GCMC scheme where nanoparticles start getting introduced into the system. After around 2×10^5 MCSs, the system morphology is observed to remain the same. With the increase in the value of ϵ_n, the system becomes very dense. Therefore, the systems seem to be stuck in some kinetically arrested states for $\epsilon_n > 0$. This can be seen in Figure 2, which shows the evolution of the number of nanoparticles in the simulation box with MCSs for: (a) $\epsilon_n = 0$; and (b) $\epsilon_n = 2k_BT$. After some MCSs, the number of nanoparticle and energy graphs show a very slow increase in its value for $\epsilon_n = 2k_BT$ in Figures 3b and 2b, respectively. Only for $\epsilon_n = 0$, the system shows a stable value of energy and the number of nanoparticles as shown in Figures 2a and 3a. Therefore, the systems with higher values of ϵ_n seem to be in a kinetically arrested state. However, for each of the values of ϵ_n, the ten independent runs converge to the same value of energy and morphological structure.

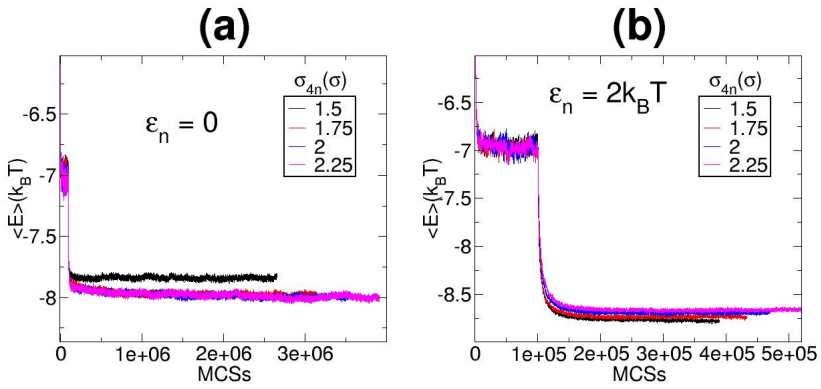

Figure 2. The figure shows the evolution of the average energy of the system with Monte Carlo steps for the values: (**a**) $\epsilon_n = 0$; and (**b**) $\epsilon_n = 2\ k_BT$. Each figure shows graphs for four different values of $\sigma_{4n} = 1.5\sigma$, 1.75σ, 2σ and 2.25σ. All graphs show a jump in their values at 10^5 Monte Carlo steps indicating the start of GCMC scheme.

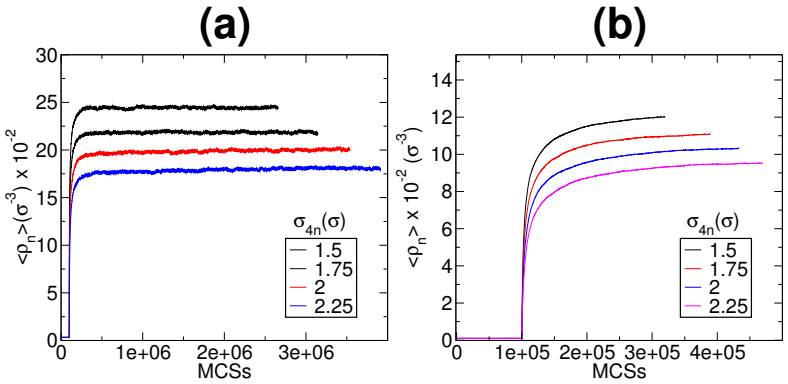

Figure 3. The figure shows the evolution of the volume fraction of nanoparticles with Monte Carlo steps for values: (**a**) $\epsilon_n = 0$; and (**b**) $\epsilon_n = 2\ k_BT$. Each figure shows the graphs of nanoparticle volume fraction for four different values of $\sigma_{4n} = 1.5\sigma$, 1.75σ, 2σ and 2.25σ. All graphs show a jump at 10^5 Monte Carlo steps when the GCMC scheme is switched on.

The observed behavior is found to be similar for $\rho_m = 0.074\sigma^{-3}$, $0.093\sigma^{-3}$ and $0.126\sigma^{-3}$. Therefore, only the snapshots for $\rho_m = 0.093\sigma^{-3}$ are used here to illustrate the behavior for all these densities. Few snapshots for illustration for other densities are also shown at the end. Figures 4 and 5 show the snapshots for values of $\epsilon_n = 2k_BT$ and $11k_BT$, respectively. Each figure shows snapshots for different values of σ_{4n} increasing from(a–d) (or (e–h)). The upper row shows both the micelles (red particles) and nanoparticle (blue), while the lower row shows only nanoparticles. For the size of nanoparticle $\sigma_n = 1.5\sigma$ considered here, the minimum value of σ_{4n} is 1.25σ [47]. For this value of $\sigma_{4n} = 1.25\sigma$, the micellar chains and nanoparticles form a uniformly mixed state (Figures 4a and 5a). No two micellar chains are found without nanoparticles in between (i.e., no clustering of chains). An increase in the value of σ_{4n} from 1.25σ leads to the formation of clusters of micellar chains that forms a network-like structure as shown in Figures 4b and 5b. Therefore, nanoparticles in (Figures 4f and 5f) are also forming network-like structures. With further increase in the value of σ_{4n}, the nanoparticle network start breaking (Figures 4g and 5g) and finally the network of nanoparticles breaks into individual clusters (Figures 4h and 5h).

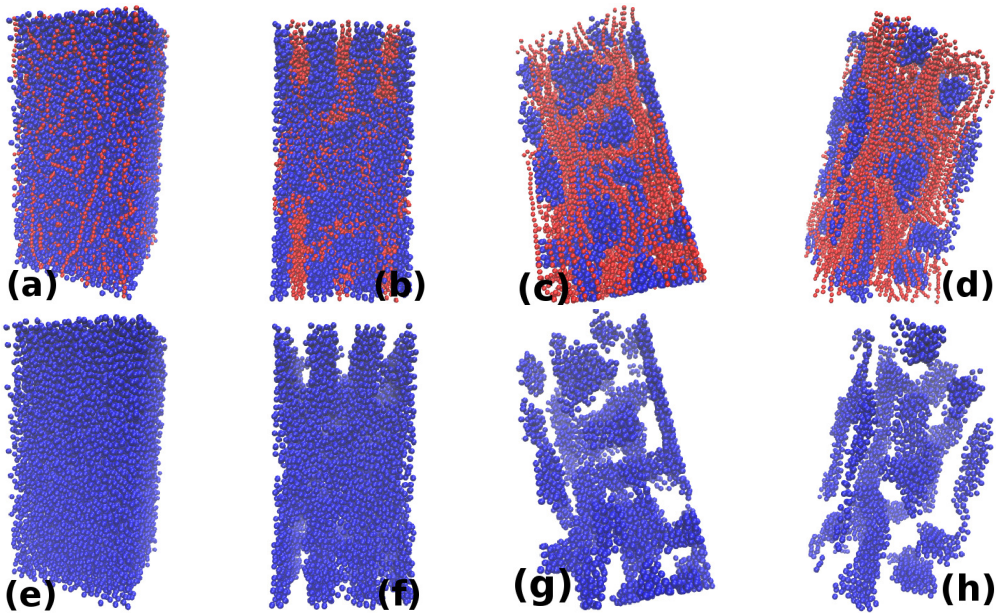

Figure 4. The figure shows snapshots for four different values of σ_{4n}: (**a**) 1.25σ; (**b**) 1.75σ; (**c**) 2.5σ; and (**d**) 2.75σ for $\epsilon_n = 2k_BT$. The upper row shows both the nanoparticles and monomers, while the lower row shows only nanoparticles. For $\sigma_{4n} = 1.25\sigma$, the micellar chains form a dispersed state. For $\sigma_{4n} > 1.25\sigma$, the nanoparticles and micellar chains form interpenetrating network-like structures which show a morphological transition for $\sigma_{4n} = 2.75\sigma$ forming individual sheets of nanoparticles.

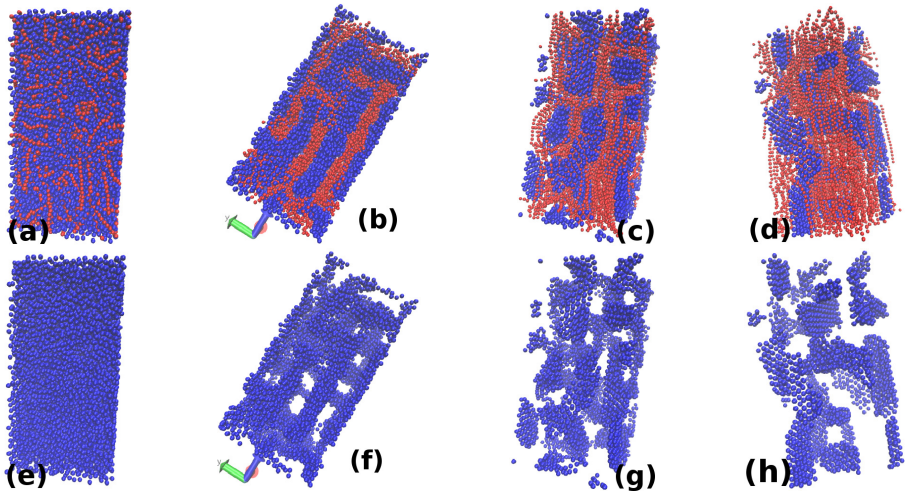

Figure 5. The figure shows snapshots for four different values: σ_{4n} is $1.25\sigma, 2\sigma, 2.5\sigma$ and 3σ in (**a**–**d**), σ_{4n} is $1.25\sigma, 2\sigma, 2.5\sigma$ and 3σ in (**e**–**h**), respectively, for $\epsilon_n = 11k_BT$. The upper row shows both the nanoparticles and monomers, while the lower row shows only nanoparticles. The polymeric chains at $\sigma_{4n} = 1.25\sigma$ form a dispersed state. For $\sigma_{4n} > 1.25\sigma$, the nanoparticles and micellar chains form interpenetrating networks which show a morphological change for $\sigma_{4n} = 2.75\sigma$ forming individual sheets of nanoparticles.

Similar morphological changes are observed for other values of ρ_m, but with a difference in the anisotropy of nanoparticle clusters. For $\rho_m = 0.093\sigma^{-3}$, the nanoparticles form sheet-like structures, while, for $\rho_m = 0.126\sigma^{-3}$, rod-like nanoparticle clusters are observed. However, irrespective of the value of ϵ_n, similar morphological transitions are observed for all ϵ_n. This shows that changes in the morphology of the structures are due to change in σ_{4n} only. Moreover, the sheet-like morphology of the structures formed in Figures 4h and 5h verifies the previous result that the micellar density governs the

morphology of nanoparticle structures. For $\epsilon_n = 0$, however, without attractive interaction between nanoparticles, a nanostructure cannot be formed; it only shows the arrangement of nanoparticles mediated by the micellar matrix. Thus, the value of ϵ_n does not seem to be affecting the morphological behavior of the system. However, the change in ϵ_n affects two things: the value of σ_{4n} at which the morphological change in nanoparticle structure occurs and the packing of nanoparticles.

Examining the Figures 4 and 5, we see that the value of σ_{4n} at which the nanoparticles undergo a transition from network-like morphology to individual clusters of nanoparticles, gets shifted to a higher value of σ_{4n} with an increase in ϵ_n. For $\epsilon_n = 0$, the breaking of network into individual clusters occurs at $\sigma_{4n} = 2.5\sigma$ (see the Supplementary Materials), but this happens at $\sigma_{4n} = 2.75\sigma$ and 3σ for the value of $\epsilon_n = 2k_BT$ (or $5k_BT$) and $11k_BT$, respectively (Figures 4h and 5h). This is because nanoparticle density increases with an increase in ϵ_n, but decreases with an increase in the value of σ_{4n}. Therefore, to reach the low nanoparticle density required to produce individual clusters, systems with a higher value of ϵ_n need to get higher values of σ_{4n}. Although the value of EVP for change in nanoparticle structure gets shifted, the value of EVP for the change in micellar chains structure from dispersed state to the formation of clusters (for $\sigma_{4n} = 1.25\sigma$ to 1.5σ) does not change with the change in ϵ_n.

An increase in the value of σ_{4n} demands an increase in the excluded volume of the system. Therefore, with increase in σ_{4n} from 1.25σ to 1.5σ, the system reorganizes itself to lower its excluded volume due to both V_4 and V_{4n}. This reorganization evokes a competition between the excluded volume due to V_4 and the excluded volume due to V_{4n}. When the value of σ_{4n} increases from 1.25σ to 1.5σ, then the micellar chains reorganizes to form clusters to decrease V_{4n}, but increasing V_4. This is because the number (or energy) of nanoparticles is higher than monomers (as shown in the following sections). When the value of σ_{4n} increases to a high value such that decreasing the distance between chains is more costly in terms of energy, then the nanoparticle density is decreased and the nanoparticle network starts breaking. When the nanoparticle network breaks to an extent that micellar chains get enough volume to be away from each other's repulsive interaction (V_4) range ($2^{1/6}\sigma_4$), then the total excluded volume of the system decreases. This change in the distance between micellar chains can be confirmed by plotting the pair correlation function. This is shown in Figure 6a.

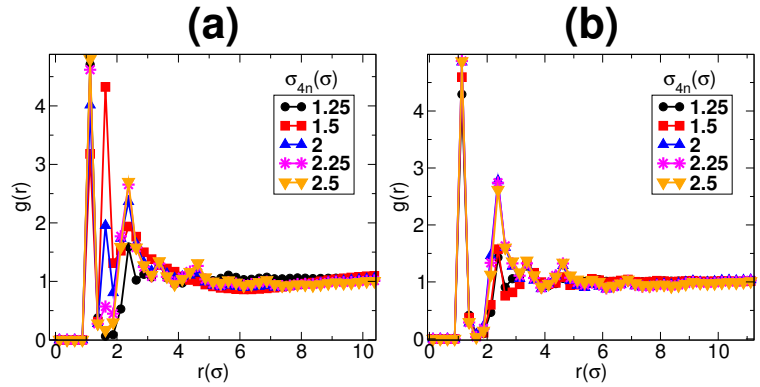

Figure 6. The figure shows the pair correlation function of monomers for values of ϵ_n: (**a**) $2k_BT$; and (**b**) 0. Each figure shows five different graphs for values of $\sigma_{4n} = 1.25\sigma$, 1.5σ, 2σ, 2.25σ and 2.5σ. A peaks around 1.75σ indicates clustering of micellar chains. For $\epsilon_n = 8k_BT$, there appear peaks around 1.75σ, which decreases with increase in σ_{4n}. However, there are no peaks around 1.75σ for $\epsilon_n = 0$.

The Figure 6a shows plots of monomer pair correlation function for $\epsilon_n = 2k_BT$. The behavior of the pair correlation function for monomers is similar for all $\epsilon_n > 0$. Figure 6a shows graphs for five different values of $\sigma_{4n} = 1.25\sigma$, 1.5σ, 2σ, 2.25σ and 2.5σ. For monomer pair correlation function, a first peak is expected at $\approx \sigma$ and its multiples indicating the monomers which are part of a chain. Peaks are also expected to occur at 1.75σ and its multiples if the chains are within the range of repulsive potential V_4. In the figure, the pair correlation function for $\sigma_{4n} = 1.25\sigma$ does not show any peak around

1.75σ. This shows that the chains are dispersed in between nanoparticles, as shown in the snapshots in Figures 4a and 5a. With the increase in σ_{4n} from 1.25σ, there appear peaks around 1.75σ and its multiples. This indicates the formation of clusters of micellar chains that join to form a network, as shown in Figures 4b and 5b. However, this peak decreases in its height with the increase in σ_{4n}. This decrease is due to the decrease in the density of nanoparticles or breaking of the nanoparticle network that decreases the excluded volume between micellar chains. For $\sigma_{4n} = 2.75\sigma$, the network breaks to an extent that micellar chains get enough volume to be out of the range of the repulsive interaction (V_4) from each other.

If nanoparticle energy is lower (-ve)than micellar chains, then an increase in σ_{4n} will lead to more clustering of micellar chains such that the distance between micellar chains decreases while the distance between micellar chains and nanoparticles increases (micellar chains are "pushed" by nanoparticles). However, if nanoparticle energy is higher, then nanoparticle density decreases without any decrease in the distance between micellar chains. This competition between the energies of nanoparticles and micellar chains can be clearly observed by examining the pair correlation functions for different values of ϵ_n. Figure 6b represents the monomer pair correlation function for $\epsilon_n = 0$. Comparing Figure 6a,b, we can clearly see that there are no peaks around 1.75σ for $\epsilon_n = 0$. This clearly shows that the energy of nanoparticles in case of $\epsilon_n = 0$ is not competitive with monomers and, hence, micellar chains do not form clusters. Therefore, for $\epsilon_n = 0$, with the increase in σ_{4n}, the number of nanoparticles decreases (or the nanoparticle network breaks) without decreasing the distance between micellar chains.

Thus, we see that, with the increase in σ_{4n}, the total excluded volume of the system increases, as a result of which the system reorganizes itself. Therefore, it is realized that the behavior of the system can be explained well if we take into account the excluded volume in the system. To take into account the excluded volume, the volume of the matrix polymeric chains are described along with the excluded volume which we call as the effective volume of micelles (or monomers). The effective volume of monomers ${V_m}^{eff}$ is defined as the total excluded volume due to repulsive interactions between chains of monomers V_4 and in between the monomers and nanoparticles V_{4n} in addition to the volume of monomers. The scheme to calculate the effective volume of micelles (or EPs) is shown in Figure 7. The figure shows that any two micellar chains at a distance $r < \sigma_4$ (σ_4, the cutoff distance for V_4) are considered as cylinders of diameter σ_4, while any monomer at a distance $r < \sigma_{4n}$ (σ_{4n}, cutoff distance for V_{4n}) is considered as a sphere of radius $\sigma_{4n} - \sigma_n/2$.

To calculate the effective volume of matrix polymers, a suitable algorithm is used to first sort out monomers which are part of a single chain. Then, all chains involved in the repulsive interaction V_4 with other chains or repelling a nanoparticle with V_{4n} are found. Then, using the scheme explained in Figure 7, the effective volume of chains is calculated. This effective volume not only depends on the value of σ_{4n} but also on the arrangement of the constituent particles that determines the number of pairs of particles repelling each other. This, in turn, depends on the density of nanoparticles. Using the scheme shown in Figure 7, the effective monomer volume fraction might be slightly overestimated, but that is insignificant and does not affect the results.

The behavior of the effective volume fraction of monomers and nanoparticles is shown in Figure 8a,b, respectively. Each graphs shows different values of ϵ_n. It should be noted that for a given value of σ_{4n}, a high value of the effective volume of monomers indicates the presence of a large number of pairs of particles having repulsive interactions between monomer chains or between monomers and nanoparticles. In Figure 8a, the effective volume shows an increase in its value with an increase in σ_{4n} from 1.25σ, representing the change from a dispersed state of chains to its clusters. Then, it shows a decrease in its value for further increase in σ_{4n} for all the values of ϵ_n except $\epsilon_n = 11k_BT$. A decrease in the value of ${V_m}^{eff}$ shows the breaking of nanoparticle network to the extent that micellar chains get enough volume to be away from each other's repulsive interaction range. We see that only for $\epsilon_n = 11k_BT$, the value of effective volume keeps on increasing with an increase in σ_{4n} and then shows a decrease at a higher value of $\sigma_{4n} = 3\sigma$. The changes in ${V_m}^{eff}$ are insignificant for $\epsilon_n = 0$ and it shows a nearly constant low value of ${V_m}^{eff}$. This confirms that, in the case of $\epsilon_n = 0$, an increase in σ_{4n}

leads to a decrease in the number of nanoparticles without decreasing the distance between micellar chains. In the graphs for nanoparticle volume fraction in Figure 8b, one can see that the nanoparticle volume fraction not only decreases with increase in σ_{4n} but also decreases slightly for a decrease in ϵ_n. The plots show similar values for all $\epsilon_n > 0$ but distinctly lower values for the case of $\epsilon_n = 0$. This indicates that, in the case of $\epsilon_n = 0$, the nanoparticle volume fraction is much lower than that of $\epsilon_n > 0$. Hence, the transition from network to individual clusters of nanoparticles can be reached at a much lower value in case of $\epsilon_n = 0$. As explained above, the increase in the excluded volume is because of the competition between the energies of the clusters of nanoparticles and monomer chains. Therefore, the behavior of the $V_m{}^{eff}$ can be confirmed by plotting the average energies of the nanoparticles and monomers.

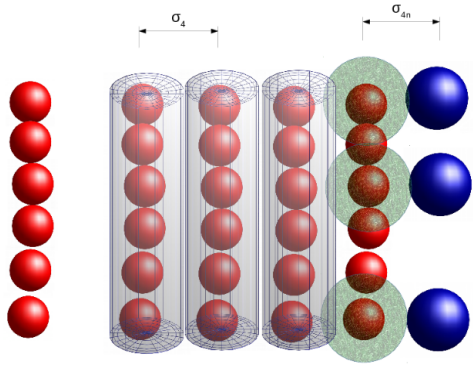

Figure 7. The figure explains the calculation of the effective volume of micelles. If any two micellar chains are at a distance $r <= \sigma_4$ from each other, they are considered as cylinders of radius $\sigma_4/2$ shown as a shaded region (red). When a nanoparticle is at a distance $r <= \sigma_{4n}$ from a monomer, then the monomer is assumed as a sphere of radius $\sigma_{4n} - \sigma_n/2$.

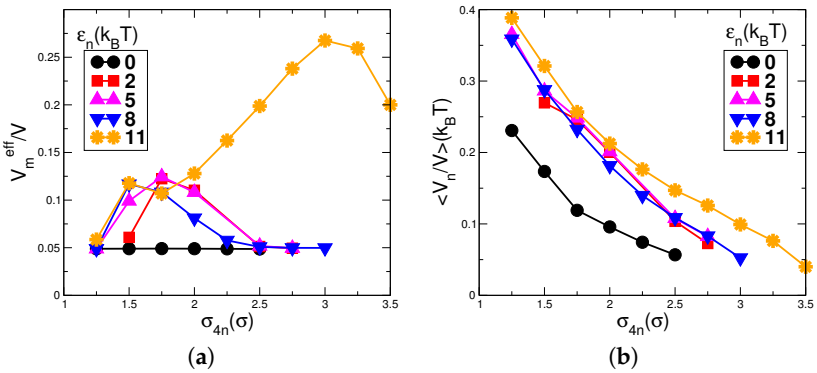

Figure 8. (**a**) The effective volume fraction of monomers; and (**b**) volume fraction of nanoparticles. The effective volume of micelles shows an increase in its value with an increase in σ_{4n} marking the change from a dispersed state to the formation of clusters of chains. With further increase in σ_{4n}, it decreases for all values of ϵ_n except for $\epsilon_n = 11k_BT$ indicating the presence of a high competition between the clusters of nanoparticles and monomer chains. The changes in $\epsilon_n = 0$ are of the very low order of magnitude and appear to be constant in this graph. The nanoparticle volume fraction shows a decreasing behavior with an increase in the value of σ_{4n} for all the values of ϵ_n. For $\epsilon_n = 0$, the values of nanoparticle volume fractions are lower than the values for other ϵ_n.

The plots of average energies of monomers and nanoparticles are shown in Figure 9a,b, respectively. Figure 9c shows the plots for both the energies simultaneously. Each figure represents graphs for different values of ϵ_n. Except for $\epsilon_n = 0$, all other values of ϵ_n indicate the two transformation points in the morphology of the system by showing a non-monotonic behavior in

Figure 9a.With the increase in σ_{4n} from 1.25σ to a higher value, the monomer energy shows an increase in its value while the nanoparticle energy shows a decrease in its value. The increase in energy of monomers is due to the increased repulsive interaction between chains due to clustering of monomer chains. This point corresponds to the transformation from a dispersed state of chains to network-like structures. With further increase in σ_{4n} the nanoparticle network breaks (volume fraction of nanoparticle decreases). Due to the breaking of the network, the available volume for monomer chains increase and hence their distance from each other increases, which results in a decrease in their repulsive interaction. Hence, the monomer energy shows a decrease (more -ve) in its value. For a higher value of σ_{4n} (depending on ϵ_n), the energy of monomers again show an increase. This increase in energy is due to a decrease in the effective volume of monomers because of the breaking of the nanoparticle network. This leads to a lower chain length of monomers hence increasing their energy [47]. Comparing the energies of monomers and nanoparticles, it can be seen that only the values of energies of monomers and nanoparticles for $\epsilon_n = 11k_BT$ are relatively comparable. For lower values of ϵ_n, nanoparticle energy is higher compared to monomers, as shown in Figure 9c, and the gap between them increases with the decrease in ϵ_n. This confirms the observed behavior of the effective volume of monomers for different values of ϵ_n shown in Figure 8a.

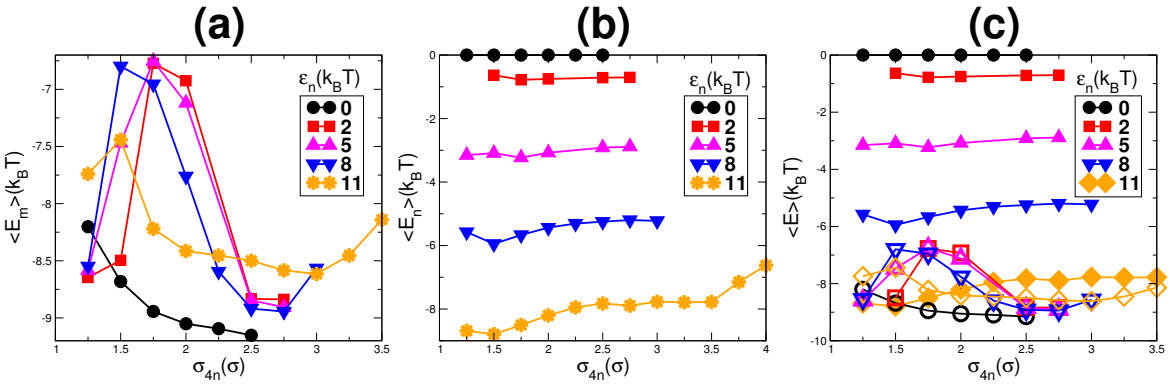

Figure 9. The average energy of: (**a**) monomers; (**b**) nanoparticles; and (**c**) both (monomers are empty symbols and nanoparticles are filled symbols). Comparing the two energies, it can be seen that only for $\epsilon_n = 11k_BT$, the energies of monomers and nanoparticles are competitive. For other values of ϵ_n, the gap between the energies is higher, as shown in (**c**).

Apart from the shift in the morphological transformation point (the value of EVP) with the change in ϵ_n, one more change with the change in ϵ_n can be easily noticed. With the decrease in the value of ϵ_n, the nanoparticle packing decreases. To gain insight into the arrangement of nanoparticles, the pair correlation function g(r) for nanoparticles is plotted in Figure 10. It shows the pair correlation function for nanoparticles with $\sigma_{4n} = 2.5\sigma$ and different values of $\epsilon_n = 0$, $2k_BT$, $5k_BT$ and $11k_BT$, as indicated by the symbols. With the decrease in ϵ_n, the height of the peak decreases. For $\epsilon_n = 0$, the peaks are broader and have a relatively short range of correlation. Hence, the packing of the nanoparticles is lowest in the case of $\epsilon_n = 0$.

As shown above [47], the same kind of behavior is shown by all densities of micelles, $\rho_m = 0.074\sigma^{-3}$, $0.093\sigma^{-3}$ and $0.126\sigma^{-3}$ except for $\rho_m = 0.037\sigma^{-3}$. In the case of $\rho_m = 0.037\sigma^{-3}$, a change in σ_{4n} from 1.25σ to 1.5σ leads to the clustering of micellar chains which joins to form a network-like structure similar to other densities. However, no change from the network to individual clusters of nanoparticles is observed for this micellar density. For all values of $\sigma_{4n} > 1.25\sigma$, the system shows the formation of a network of nanoparticle clusters and micellar chains with no further structural change observed for any value of σ_{4n} considered here. This is true for all ϵ_n considered here. A comparison of the systems with $\rho_m = 0.037\sigma^{-3}$ for different values of ϵ_n is shown in Supplementary Materials. The systems for $\rho_m = 0.037\sigma^{-3}$ are also reproduced in a bigger box size of $60 \times 60 \times 60\sigma^3$ to check the simulation artefacts. One of the snapshots for $\sigma_{4n} = 2.75\sigma$ and $\epsilon_n = 0$ is shown in

Figure 11a,b. The snapshot in Figure 11a shows the nanoparticles (blue) and micelles (red) both while, only nanoparticles from the snapshot in Figure 11a are shown in Figure 11b. The snapshots show the network of nanoparticle clusters interpenetrating with the network of micellar chains.

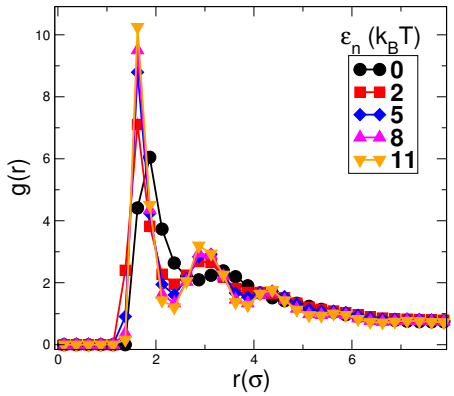

Figure 10. The figure shows the pair correlation function for nanoparticles with $\sigma_{4n} = 2.5\sigma$ and for different values of ϵ_n. The height of the peaks decreases with the decrease in ϵ_n. The lowest and broader peak for $\epsilon_n = 0$ shows that the nanoparticle packing, in this case, is lowest.

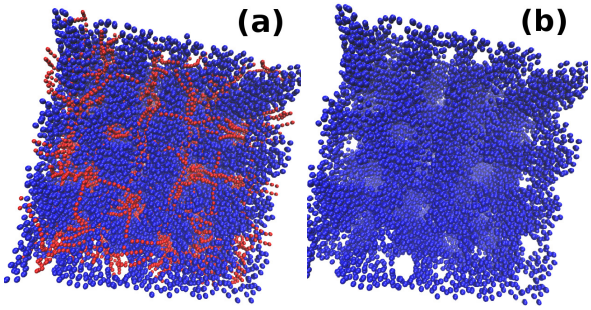

Figure 11. Snapshots for $\rho_m = 0.037\sigma^{-3}, \epsilon_n = 0, \sigma_{4n} = 2.75\sigma$ reproduced in a larger box size of $60 \times 60 \times 60\sigma^3$: (**a**) both the nanoparticles (blue) and monomers (red); and (**b**) only nanoparticles. The structure obtained for the larger box size are similar to smaller box size shown in Supplementary Materials.

Throughout the paper, the value of the size of nanoparticles is kept constant at $\sigma_n = 1.5\sigma$. For the range of values of σ_{4n} considered, no change from network to individual clusters for nanoparticles is observed for the value of $\rho_m = 0.037\sigma^{-3}$. However, for nanoparticle size $\sigma_n = 3\sigma$, the transition occurs at the value of $\sigma_{4n} = 3.25\sigma$ for the value of $\epsilon_n = 0$. While keeping the other parameters same but increasing ϵ_n to $11k_BT$, a percolating network of nanoparticles is observed. This is another example of the shift in the value of EVP for the system morphological change with the change in ϵ_n. This is shown in Figure 12. It is interesting to note that the snapshot in Figure 12a shows system spanning sheets of nanoparticles (arranged in alternate layers of nanoparticles and micellar chains). Apart from that, the arrangement or packing of nanoparticles is relatively low in Figure 12a compared to Figure 12b. A similar example is shown in Figure 13. It shows two snapshots for: (a) $\epsilon_n = 0$; and (b) $\epsilon_n = 11k_BT$, keeping the values of $\rho_m = 0.126\sigma^{-3}$ and $\sigma_{4n} = 2.25\sigma$ and $\sigma_n = 1.5\sigma$ the same for both. The system with this micellar No. density $\rho_m = 0.126\sigma^{-3}$ is shown to be produce rod-like morphology of nanoparticle clusters [47]. Here, the snapshots are shown for the value of σ_{4n} past the point of transformation from network to individual clusters. Hence, the systems are showing rodlike structures of nanoparticles. However, the rods in case of $\epsilon_n = 0$ (in Figure 13c) can be seen as thinner compared to the rods in Figure 13d for $\epsilon_n = 11k_BT$. Moreover, one can clearly see the difference in the packing of nanoparticles. The nanoparticles are well packed in Figure 13d compared to Figure 13c.

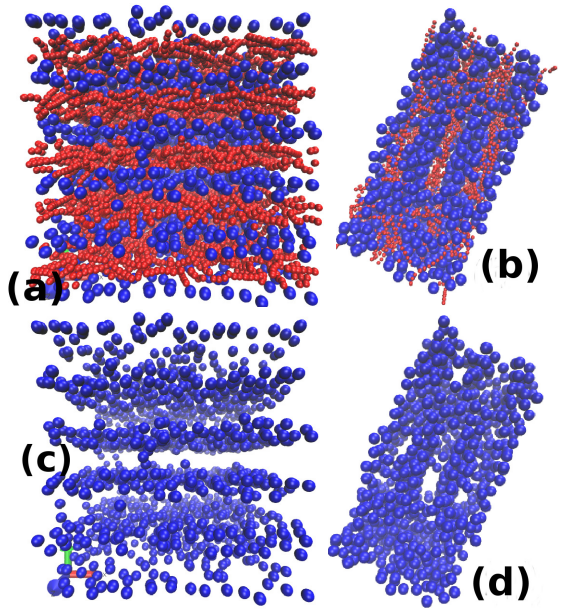

Figure 12. Snapshots for $\rho_m = 0.037\sigma^{-3}, \sigma_n = 3\sigma, \sigma_{4n} = 3.25\sigma$ for two different values of ϵ_n: (**a**) 0; and (**b**) $11k_BT$. The upper row shows both the nanoparticles and monomers, while the lower row only shows the nanoparticles. The point of the structural change for nanoparticles gets shifted to lower values of σ_{4n} with a decrease in ϵ_n. Therefore, the left snapshots show a system forming system spanning sheet of nanoparticles while the right figure is still in the regime of percolating network-like structure despite having the same values of σ_{4n}.

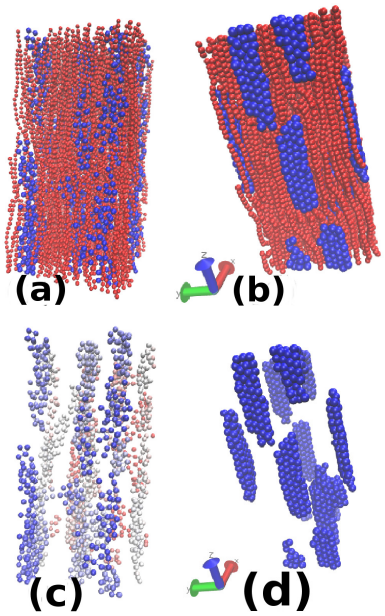

Figure 13. Snapshots for the $\rho_m = 0.126\sigma^{-3}$ and $\sigma_{4n} = 2\sigma$: (**a**) $\epsilon_n = 0$; and (**b**) $\epsilon_n = 11\ k_BT$. The upper row only shows both the nanoparticles (blue) and micelles (red) while the lower row only shows nanoparticles. Only (**c**) has a gradient in its colour along one of the shorter axes of the box. Comparison of both the figure shows that a lower value of ϵ_n leads to low volume fraction and low packing of nanoparticles. Therefore the rods formed in (**c**) do not show a well-packed structure compared to the right figure and are also thinner.

4. Conclusion

A detailed investigation of the effect of the strength of interaction between nanoparticles on the structural behavior of the Wormlike micelles-nanoparticles system is carried out. It is shown that with the decrease in the value of ϵ_n, the point (value of EVP) of the transition from network to individual clusters of nanoparticles gets shifted to the lower value of σ_{4n}. It is also shown that this shift in transition point is due to a decrease in the nanoparticle volume fraction with the decrease in ϵ_n. For the case of $\epsilon_n = 0, \sigma_n = 3\sigma$ and $\sigma_{4n} = 3.25\sigma$, system spanning sheet-like arrangement of nanoparticles is reported. The investigation also shows that a decrease in the value of ϵ_n leads to a decrease in the packing of nanoparticles.

Supplementary Materials: Supplementary Materials can be found at: www.mdpi.com/2410-3896/3/4/31/s1.

Funding: This research received no external funding.

Acknowledgments: We thank the computational facility provided National Param Super Computing (NPSF) CDAC, India for use of Yuva cluster, the computer cluster in IISER-Pune, funded by DST, India by Project No. SR/NM/NS-42/2009.

Conflicts of Interest: The authors declare no conflict of interest.

References

1. Bisquert, J. *Nanostructured Energy Devices: Foundations of Carrier Transport*; CRC Press: Boca Raton, FL, USA, 2017.
2. Daubinger, P. Hierarchical Nanostructures for Energy Devices. *Johnson Matthey Technol. Rev.* **2016**, *60*. [CrossRef]
3. Yi, G.C. *Semiconductor Nanostructures for Optoelectronic Devices: Processing, Characterization and Applications*; Springer: Berlin, Germany, 2012.
4. Domènech, B.; Muñoz, M.; Muraviev, D.; Macanás, J. Polymer-Silver nanocomposites as antibacterial materials. In *Microbial Pathogens and Strategies for Combating Them: Science, Technology and Education*; Méndez-Vilas, A., Ed.; Formatex Research Center: Badajoz, Spain, 2013.
5. Sambarkar, P.; Patwekar, S.; Dudhgaonkar, B. Polymer nanocomposites: An overview. *Int. J. Pharm. Pharm. Sci.* **2012**, *4*, 60–65.
6. Ray, S.S.; Bousmina, M. *Polymer Nanocomposites and Their Applications*; Scientific American: New York, NY, USA, 2006.
7. Arraudeau, J.; Patraud, J.; Gall, L. Composition Based on Cationic Polymers, Anionic Polymers and Waxes for Use in Cosmetics. U.S. Patent 4,871,536, 3 October 1989.
8. Tatum, J.P.; Wright, R.C. Organoclay Materials. U.S. Patent 4,752,342, 21 June 1988.
9. Sorrentino, A.; Gorrasi, G.; Vittoria, V. Potential perspectives of bio-nanocomposites for food packaging applications. *Trends Food Sci. Technol.* **2007**, *18*, 84–95. [CrossRef]
10. De Azeredo, H.M. Nanocomposites for food packaging applications. *Food Res. Int.* **2009**, *42*, 1240–1253. [CrossRef]
11. Ingrosso, C.; Panniello, A.; Comparelli, R.; Curri, M.L.; Striccoli, M. Colloidal inorganic nanocrystal based nanocomposites: Functional materials for micro and nanofabrication. *Materials* **2010**, *3*, 1316–1352. [CrossRef]
12. Segala, K.; Pereira, A.S. From Ruthenium Complexes to Novel Functional Nanocomposites: Development and Perspectives. In *New Polymers for Special Applications*; InTech: Garching, Germany, 2012.
13. Seul, M.; Andelman, D. Domain shapes and patterns: the phenomenology of modulated phases. *Science* **1995**, *267*, 476. [CrossRef] [PubMed]
14. Tang, Z.; Zhang, Z.; Wang, Y.; Glotzer, S.C.; Kotov, N.A. Self-assembly of CdTe nanocrystals into free-floating sheets. *Science* **2006**, *314*, 274–278. [CrossRef] [PubMed]
15. Miyashita, T. Fabrication of Soft Nano-devices using Polymer Nano-sheets. *J. Netw. Polym. Jpn.* **2004**, *25*, 34–43.
16. Black, C.; Guarini, K.; Breyta, G.; Colburn, M.; Ruiz, R.; Sandstrom, R.; Sikorski, E.; Zhang, Y. Highly porous silicon membrane fabrication using polymer self-assembly. *J. Vacuum Sci. Technol. B* **2006**, *24*, 3188–3191. [CrossRef]

17. Orski, S.V.; Fries, K.H.; Sontag, S.K.; Locklin, J. Fabrication of nanostructures using polymer brushes. *J. Mater. Chem.* **2011**, *21*, 14135–14149. [CrossRef]
18. Shenhar, R.; Norsten, T.B.; Rotello, V.M. Polymer-Mediated Nanoparticle Assembly: Structural Control and Applications. *Adv. Mater.* **2005**, *17*, 657–669. [CrossRef]
19. Hamley, I. Nanostructure fabrication using block copolymers. *Nanotechnology* **2003**, *14*, R39. [CrossRef]
20. Asakura, S.; Oosawa, F. On interaction between two bodies immersed in a solution of macromolecules. *J. Chem. Phys.* **1954**, *22*, 1255–1256. [CrossRef]
21. Asakura, S.; Oosawa, F. Interaction between particles suspended in solutions of macromolecules. *J. Polym. Sci.* **1958**, *33*, 183–192. [CrossRef]
22. Reister, E.; Fredrickson, G.H. Phase behavior of a blend of polymer-tethered nanoparticles with diblock copolymers. *J. Chem. Phys.* **2005**, *123*, 214903. [CrossRef] [PubMed]
23. Sides, S.W.; Kim, B.J.; Kramer, E.J.; Fredrickson, G.H. Hybrid particle-field simulations of polymer nanocomposites. *Phys. Rev. Lett.* **2006**, *96*, 250601. [CrossRef] [PubMed]
24. Detcheverry, F.A.; Kang, H.; Daoulas, K.C.; Müller, M.; Nealey, P.F.; de Pablo, J.J. Monte Carlo simulations of a coarse grain model for block copolymers and nanocomposites. *Macromolecules* **2008**, *41*, 4989–5001. [CrossRef]
25. Beecroft, L.L.; Ober, C.K. Nanocomposite materials for optical applications. *Chem. Mater.* **1997**, *9*, 1302–1317. [CrossRef]
26. Kumar, S.K.; Krishnamoorti, R. Nanocomposites: Structure, phase behavior, and properties. *Annu. Rev. Chem. Biomol. Eng.* **2010**, *1*, 37–58. [CrossRef] [PubMed]
27. Chao, H.; Riggleman, R.A. Effect of particle size and grafting density on the mechanical properties of polymer nanocomposites. *Polymer* **2013**, *54*, 5222–5229. [CrossRef]
28. Koski, J.; Chao, H.; Riggleman, R.A. Field theoretic simulations of polymer nanocomposites. *J. Chem. Phys.* **2013**, *139*, 244911. [CrossRef] [PubMed]
29. Lee, J.Y.; Balazs, A.C.; Thompson, R.B.; Hill, R.M. Self-Assembly of Amphiphilic Nanoparticle-Coil "Tadpole" Macromolecules. *Macromolecules* **2004**, *37*, 3536–3539. [CrossRef]
30. Balazs, A.C.; Singh, C.; Zhulina, E. Modeling the interactions between polymers and clay surfaces through self-consistent field theory. *Macromolecules* **1998**, *31*, 8370–8381. [CrossRef]
31. Thompson, R.B.; Ginzburg, V.V.; Matsen, M.W.; Balazs, A.C. Block copolymer-directed assembly of nanoparticles: Forming mesoscopically ordered hybrid materials. *Macromolecules* **2002**, *35*, 1060–1071. [CrossRef]
32. Hore, M.J.; Frischknecht, A.L.; Composto, R.J. Nanorod assemblies in polymer films and their dispersion-dependent optical properties. *ACS Macro Lett.* **2011**, *1*, 115–121. [CrossRef]
33. Frischknecht, A.L.; Hore, M.J.; Ford, J.; Composto, R.J. Dispersion of polymer-grafted nanorods in homopolymer films: Theory and experiment. *Macromolecules* **2013**, *46*, 2856–2869. [CrossRef]
34. McGarrity, E.; Frischknecht, A.; Mackay, M. Phase behavior of polymer/nanoparticle blends near a substrate. *J. Chem. Phys.* **2008**, *128*, 154904. [CrossRef] [PubMed]
35. De Pablo, J.J. Coarse-grained simulations of macromolecules: From DNA to nanocomposites. *Ann. Rev. Phys. Chem.* **2011**, *62*, 555–574. [CrossRef] [PubMed]
36. Riggleman, R.A.; Toepperwein, G.; Papakonstantopoulos, G.J.; Barrat, J.L.; de Pablo, J.J. Entanglement network in nanoparticle reinforced polymers. *J. Chem. Phys.* **2009**, *130*, 244903. [CrossRef] [PubMed]
37. Kang, H.; Detcheverry, F.A.; Mangham, A.N.; Stoykovich, M.P.; Daoulas, K.C.; Hamers, R.J.; Müller, M.; de Pablo, J.J.; Nealey, P.F. Hierarchical assembly of nanoparticle superstructures from block copolymer-nanoparticle composites. *Phys. Rev. Lett.* **2008**, *100*, 148303. [CrossRef] [PubMed]
38. Louis, A.; Bolhuis, P.; Hansen, J.; Meijer, E. Can polymer coils be modeled as "soft colloids"? *Phys. Rev. Lett.* **2000**, *85*, 2522. [CrossRef] [PubMed]
39. Bolhuis, P.; Louis, A.; Hansen, J. Influence of polymer-excluded volume on the phase-behavior of colloid-polymer mixtures. *Phys. Rev. Lett.* **2002**, *89*, 128302. [CrossRef] [PubMed]
40. Bolhuis, P.G.; Meijer, E.J.; Louis, A.A. Colloid-polymer mixtures in the protein limit. *Phys. Rev. Lett.* **2003**, *90*, 068304. [CrossRef] [PubMed]
41. Bagwe, R.P.; Hilliard, L.R.; Tan, W. Surface modification of silica nanoparticles to reduce aggregation and nonspecific binding. *Langmuir* **2006**, *22*, 4357–4362. [CrossRef] [PubMed]

42. Mendoza, C.I.; Batta, E. Self-assembly of binary nanoparticle dispersions: From square arrays and stripe phases to colloidal corrals. *EPL* **2009**, *85*, 56004. [CrossRef]
43. Martin, T.B.; Jayaraman, A. Effect of matrix bidispersity on the morphology of polymer-grafted nanoparticle-filled polymer nanocomposites. *J. Polym. Sci. Part B Polym. Phys.* **2014**, *52*, 1661–1668. [CrossRef]
44. Nair, N.; Wentzel, N.; Jayaraman, A. Effect of bidispersity in grafted chain length on grafted chain conformations and potential of mean force between polymer grafted nanoparticles in a homopolymer matrix. *J. Chem. Phys.* **2011**, *134*, 194906. [CrossRef] [PubMed]
45. Hakem, I.F.; Leech, A.M.; Johnson, J.D.; Donahue, S.J.; Walker, J.P.; Bockstaller, M.R. Understanding ligand distributions in modified particle and particlelike systems. *J. Am. Chem. Soc.* **2010**, *132*, 16593–16598. [CrossRef] [PubMed]
46. Zhao, D.; Di Nicola, M.; Khani, M.M.; Jestin, J.; Benicewicz, B.C.; Kumar, S.K. Role of block copolymer adsorption versus bimodal grafting on nanoparticle self-assembly in polymer nanocomposites. *Soft Matter* **2016**, *12*, 7241–7247. [CrossRef] [PubMed]
47. Mubeena, S. Wormlike micelle-nanoparticles composite: A computational investigation. *arXiv* **2018**, arXiv:cond-mat.soft/1801.06933.
48. Mubeena, S.; Chatterji, A. Hierarchical self-assembly: Self-organized nanostructures in a nematically ordered matrix of self-assembled polymeric chains. *Phys. Rev. E* **2015**, *91*, 032602. [CrossRef] [PubMed]
49. Chatterji, A.; Pandit, R. The statistical mechanics of semiflexible equilibrium polymers. *J. Stat. Phys.* **2003**, *110*, 1219–1248. [CrossRef]